Modulational instability of zone boundary mode and band edge modes in nonlinear diatomic lattices

Yusuke Doi* and Akihiro Nakatani
Department of Adaptive Machine Systems, Graduate School of Engineering, Osaka University, 2-1 Yamadaoka, Suita, Osaka 565-0871, Japan

Kazuyuki Yoshimura
NTT Communication Science Laboratories, 2-4 Hikaridai, Seika-cho, Soraku-gun, Kyoto 619-0237, Japan
(Received 7 October 2008; published 4 February 2009)

We analyze the modulational instability of the zone boundary mode (ZBM) and the band edge modes (BEMs) in a one-dimensional nonlinear diatomic lattice and obtain rigorous results. Some numerical calculations of modulational instability in these modes are presented. These results indicate that the modulational instability of the BEMs leads to excitation of the discrete breathers (DBs) in the band gap, while that of the ZBM leads to excitation of the DBs above the phonon band.

DOI: 10.1103/PhysRevE.79.026603 PACS number(s): 05.45.−a

I. INTRODUCTION

Nonlinear vibrations in lattice systems have been studied for a long time. It is well known that nonlinear dynamics gives rise to various phenomena such as instability, pattern formation, and localization. These phenomena play important roles in vibration problems encountered in lattice systems.

One of the pioneering studies of nonlinear vibrations was carried out by Fermi, Pasta, and Ulam [1], in which they studied the energy relaxation in a one-dimensional anharmonic lattice called after them the Fermi-Pasta-Ulam (FPU) system. They have investigated the energy transfer between normal modes due to the nonlinearity of the system. Their purpose was to show that the nonlinearity of the system leads to thermal equilibrium by energy transfer between the normal modes. However, they could not obtain the expected result. Instead, they found energy recurrence between a few normal modes in the FPU system. Their focus was mainly on phenomena that can be connected to the continuum limit. They also focused on the behavior of normal modes having considerably longer wavelengths as compared to the lattice spacing.

Recently, vibration phenomena with short wavelengths have also been studied extensively. Takeno and co-workers reported a time-periodic and space-localized structure called a discrete breather (DB) or intrinsic localized mode (ILM) [2,3]. The DB lies outside the linear dispersion band. In the FPU lattice, the dispersion band has a single upper bound $\omega_{\max}$. Therefore, the internal frequency ω_{DB} of a DB is always higher than $\omega_{\max}$.

DBs exhibit interesting dynamics. One of the important aspects of the dynamics of DBs is their excitation process. It is known that DBs or DB-like structures called chaotic breathers (CBs) [4–7] are excited by the modulational instability of the zone boundary mode (ZBM) in lattice systems. In lattice systems, the zone boundary is above the upper boundary of the dispersion band. Thus, modulational instability is an important mechanism for the excitation of DBs in lattice systems. In fact, a direct relation between the modulational instability of the ZBM and the existence of DBs has been discussed in [8].

A lot of studies have been carried out on the modulational instability in various systems such as FPU systems [9–13] and nonlinear Klein-Gordon systems [14,15]. However, there are no rigorous results on the analysis of the modulational instability in anharmonic lattices, except for a study of the monoatomic FPU lattice by one of the authors [13].

In the present study, we focus on the diatomic FPU lattice. A diatomic lattice, which is a generalization of a monoatomic system, consists of two types of particles. Hence, the dispersion curve of a diatomic lattice has two branches: an acoustic branch and an optical branch. A gap exists between these two branches. DBs can exist in this gap [16–20]. Thus, the modulational instability of the band edge modes (BEMs) is an important mechanism for the excitation of DBs in the gap. However, the stability of the ZBM and BEMs in diatomic lattices has not been analyzed. The main objective of the present study is to obtain rigorous results from the stability analysis of the ZBM and the BEMs in a one-dimensional diatomic lattice.

This paper is organized as follows. In Sec. II, we describe the method of the stability analysis of the periodic solution of a homogeneous potential system carried out by using the Gauss hypergeometric differential equation. In Sec. III, the ZBM and the BEMs in diatomic lattice systems are derived: in these systems, the zone boundary and band edge are located just on the edge of the acoustic and optical branches, respectively. In Sec. IV, we present the rigorous results obtained from the stability analysis of the ZBM and the BEMs. Some numerical calculations of the modulational instability of these modes are also shown. Conclusions are presented in Sec. V.

II. STABILITY ANALYSIS OF PERIODIC SOLUTIONS

Consider the linear differential equation

*doi@ams.eng.osaka-u.ac.jp

$$\frac{d^2x}{dt^2} + f(t)x = 0, \tag{1}$$

where $f(t)$ is a periodic function with period T.

Let $\{x_1(t), x_2(t)\}$ be the fundamental solution of (1). A *monodromy matrix* $\mathcal{M}$ is defined as the mapping from the solution of (1) at t to the solution of (1) at $t+T$:

$$\begin{pmatrix} x_1(t+T) \\ x_2(t+T) \end{pmatrix} = \mathcal{M} \begin{pmatrix} x_1(t) \\ x_2(t) \end{pmatrix}. \tag{2}$$

Since (1) is the equation of motion of a Hamiltonian system, the eigenvalues of $\mathcal{M}$ are given by (ρ, ρ^{-1}). Hereafter, we assume $|\rho| \geqslant |\rho^{-1}|$. These eigenvalues are also called characteristic multipliers. The characteristic exponent σ is defined as $\sigma = \pm T^{-1} \ln|\rho|$. The solution $\{x_1(t), x_2(t)\}$ is unstable when σ is positive.

Next, we consider the stability of the periodic solution of the equation of a homogeneous potential system of even order given as

$$\frac{d^2\phi}{dt^2} + \alpha_{2p}\phi^{2p-1} = 0 \tag{3}$$

and

$$\frac{d^2\xi}{dt^2} + \beta_{2p}\phi^{2p-2}\xi = 0, \tag{4}$$

where $p \in \mathrm{Z}$ is positive. Equation (4) is a particular case of (1). Here, we define the *stability parameter* λ_{2p} as

$$\lambda_{2p} = \frac{\beta_{2p}}{\alpha_{2p}}. \tag{5}$$

Next, we consider the period T of the solution ϕ. Integrating (3), we obtain

$$\frac{1}{2}\left(\frac{d\phi}{dt}\right)^2 + \frac{\alpha_{2p}}{2p}\phi^{2p} = h, \tag{6}$$

where h is a positive constant. The function $\phi(t)$ is the inverse function of the integral

$$\int_{t_0}^{t} dt = \int_{\phi_0}^{\phi} \frac{dw}{\sqrt{\Pi(w)}}, \tag{7}$$

where

$$\Pi(w) = 2h - \frac{\alpha_{2p}}{p}w^{2p}. \tag{8}$$

If we consider the right-hand side (RHS) of (7) as the integral in a complex domain, there exist branch points $s_n \in \mathrm{C}$ on a Riemann surface defined by $z = \sqrt{\Pi(w)}$:

$$s_n = \left(\frac{2ph}{\alpha_{2p}}\right)^{1/2p} e^{in\pi/p} \quad (n = 0,1,2,\ldots,2p-1). \tag{9}$$

Equation (7) gives the period of $\phi(t)$ when it is integrated along a closed path. Taking γ as the closed path that involves only two branch points on the real axis, $s_0 = (2ph/\alpha_{2p})^{1/2p} \in \mathbb{R}$ and $s_p = -(2ph/\alpha_{2p})^{1/2p} \in \mathbb{R}$, we can obtain the real period T of ϕ as

$$T = \oint_{\gamma} \frac{dw}{\sqrt{2h - \frac{\alpha_{2p}}{p}w^{2p}}}. \tag{10}$$

It is well known that (4) can be transformed into the Gauss hypergeometric differential equation by the variable transformation $z = (\frac{\alpha_{2p}}{2ph})[\phi(t)]^{2p}$ [21], as follows (see Appendix A for the derivation):

$$z(1-z)\frac{d^2\xi}{dz^2} + [c - (a+b+1)z]\frac{d\xi}{dz} - ab\xi = 0, \tag{11}$$

where

$$a + b = \frac{1}{2} - \frac{1}{2p}, \quad ab = -\frac{\lambda_{2p}}{4p}, \quad c = 1 - \frac{1}{2p}. \tag{12}$$

It is possible to obtain the explicit form $\mathcal{M}$ using (11). Equation (11) has two singular points at $z=0$ and $z=1$. Let γ_0 and γ_1 be the anticlockwise closed paths around $z=0$ and $z=1$, respectively. The monodromy matrices $\mathcal{M}(\gamma_0)$ and $\mathcal{M}(\gamma_1)$ are given by

$$\mathcal{M}(\gamma_0) = \begin{pmatrix} 1 & e^{-2\pi ib} - e^{-2\pi ic} \\ 0 & e^{-2\pi ic} \end{pmatrix}, \tag{13}$$

$$\mathcal{M}(\gamma_1) = \begin{pmatrix} e^{-2\pi i(c-a-b)} & 0 \\ 1 - e^{2\pi i(c-a)} & 1 \end{pmatrix}, \tag{14}$$

for a certain set of fundamental solutions [21]. The path γ in the w plane is mapped to $\gamma_1\gamma_0^p\gamma_1\gamma_0^p$ in the z plane by the variable transformation $z = (\frac{\alpha_{2p}}{2ph})w^{2p}$. Thus, $\mathcal{M}(\gamma)$ is given by

$$\mathcal{M}(\gamma) = \mathcal{M}(\gamma_0)^p\mathcal{M}(\gamma_1)\mathcal{M}(\gamma_0)^p\mathcal{M}(\gamma_1). \tag{15}$$

Substituting (13) and (14) into (15), we obtain the explicit form of $\mathcal{M}(\gamma)$:

$$\mathcal{M}(\gamma) = \begin{pmatrix} ABC - 1 & BC \\ -A & -1 \end{pmatrix}^2, \tag{16}$$

where

$$A = 1 - e^{2\pi i(c-a)}, \tag{17}$$

$$B = 1 - e^{2\pi i(c-b)}, \tag{18}$$

$$C = \frac{2}{1 - e^{2\pi ic}}. \tag{19}$$

Next, we study the properties of $\mathcal{M}(\gamma)$. The trace of $\mathcal{M}(\gamma)$ can be expressed as

$$\mathrm{tr}\mathcal{M}(\gamma) = \frac{4}{\sin^2\left(\frac{\pi}{2p}\right)} \cos^2\left[\frac{\pi}{2p}\sqrt{(p-1)^2 + 4p\lambda_{2p}}\right] - 2$$
$$\equiv 2F_{2p}(\lambda_{2p}). \tag{20}$$

The determinant of $\mathcal{M}(\gamma)$ can also be obtained from (16),

$$|\mathcal{M}(\gamma)| = 1. \tag{21}$$

The eigenvalues $(\rho_{2p}, \rho_{2p}^{-1})$ of $\mathcal{M}(\gamma)$ are given by the solutions of the characteristic equation

$$\rho^2 - \mathrm{tr}\mathcal{M}(\gamma)\rho + 1 = 0. \tag{22}$$

From (20) and (22), we obtain $\rho_{2p}, \rho_{2p}^{-1} = F_{2p}(\lambda_{2p}) \pm \sqrt{[F_{2p}(\lambda_{2p})]^2 - 1}$. Thus, σ is given by

$$\sigma = \pm T^{-1} \ln|F_{2p}(\lambda_{2p}) \pm \sqrt{[F_{2p}(\lambda_{2p})]^2 - 1}|. \tag{23}$$

Considering Eq. (23), we find that there exists a positive σ when $F_{2p}(\lambda_{2p}) > 1$ [21]. This condition is satisfied if and only if λ_{2p} is in the region S_{2p} defined by

$$S_{2p} = s_{2p}(0) \cup s_{2p}(1) \cup s_{2p}(2) \cup \cdots, \tag{24}$$

where

$$s_{2p}(0) = \{\lambda \in \mathbb{R} | \lambda < 0\}, \tag{25}$$

$$s_{2p}(i) = \{\lambda \in \mathbb{R} | a_i < \lambda < b_i\} \quad (i = 1,2, \ldots). \tag{26}$$

The parameters a_i and b_i are defined as follows:

$$a_i = i(i-1)p + i, \tag{27}$$

$$b_i = i(i+1)p - i. \tag{28}$$

We also define the region $\bar{s}_{2p}(i)$ for later discussions as

$$\bar{s}_{2p}(i) = \{\lambda \in \mathbb{R} | b_{i-1} < \lambda < a_i\}. \tag{29}$$

III. DIATOMIC LATTICE AND ITS ZBM AND BEMS

We consider a diatomic lattice system whose Hamiltonian is written as

$$H = \frac{1}{2}\sum_{j=1}^{2N} m_j \dot{q}_j^2 + \sum_{j=1}^{2N}\sum_{r=1}^{p} \frac{K_{2r}}{2r}(q_{j+1} - q_j)^{2r}, \tag{30}$$

where $K_{2r} \in \mathbb{R}$ is a constant. We assume that $K_{2r} \geqslant 0$ and $m_j > 0$. We can set $K_2 = 1$ without loss of generality. The following periodic boundary conditions are considered:

$$q_{2N+1} = q_1, \tag{31}$$

$$\dot{q}_{2N+1} = \dot{q}_1. \tag{32}$$

The mass of each particle in the system, m_j, is given as follows:

$$m_{2j-1} = M,$$

$$m_{2j} = m \quad (j = 1,2, \ldots, N), \tag{33}$$

where $m < M$. We can set $M = 1$ without loss of generality.

The equations of the motion of the system given by (30) are

$$\ddot{q}_{2j-1} + \sum_{r=1}^{p} K_{2r}[(q_{2j-1} - q_{2j-2})^{2r-1} + (q_{2j-1} - q_{2j})^{2r-1}] = 0, \tag{34}$$

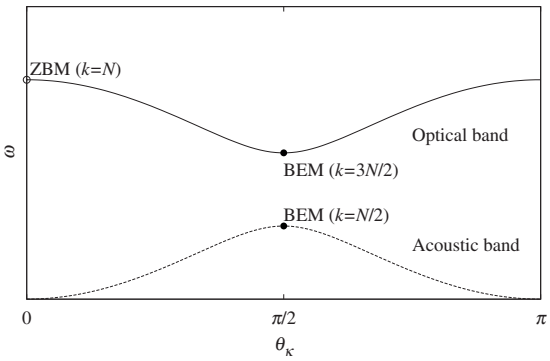

FIG. 1. Dispersion curve of diatomic lattice systems. The two black circles indicate the BEMs in acoustic and optical bands. The white circle indicates the ZBM.

$$m\ddot{q}_{2j} + \sum_{r=1}^{p} K_{2r}[(q_{2j} - q_{2j-1})^{2r-1} + (q_{2j} - q_{2j+1})^{2r-1}] = 0. \tag{35}$$

When $p = 1$, Eqs. (34) and (35) become linear equations. If we consider the linear plane waves

$$q_{2j-1} = X_1 \cos[(2j-1)\theta_\kappa]\exp(i\Omega t), \tag{36}$$

$$q_{2j} = X_2 \cos(2j\theta_\kappa)\exp(i\Omega t), \tag{37}$$

we obtain the linear dispersion relation

$$\Omega^2(\kappa, \text{branch}) = \left(1 + \frac{1}{m}\right) \pm \sqrt{\left(1 + \frac{1}{m}\right)^2 - \frac{4}{m}\sin^2\theta_\kappa}, \tag{38}$$

where κ is a wave number and θ_κ is a constant determined by the boundary conditions (31) and (32):

$$\theta_\kappa = \frac{\kappa}{N}\pi, \quad \kappa = 0,1,2, \ldots, N-1. \tag{39}$$

It is well known that the linear dispersion curve of a diatomic lattice system has two branches, as shown in Fig. 1. The signs + and − in (38) indicate the optical band (high frequency) and the acoustic band (low frequency) in the linear dispersion relation, respectively. The zone boundary is the upper bound of the optical band. The band edges are the lower and upper bounds of the optical and acoustic bands, respectively.

Here, we introduce a new variable k defined as

$$k = \begin{cases} \kappa & \text{for the acoustic branch,} \\ \kappa + N & \text{for the optical branch.} \end{cases} \tag{40}$$

In the following discussions, we can use functions that depend on k instead of those depending on κ and the type of branch. By using k, the ZBM corresponds to $k = N$. Further, the two BEMs correspond to $k = N/2$ (acoustic) and $k = 3N/2$ (optical).

By replacing Ω (κ, branch) with $\omega(k)$ in the linear dispersion relation, we obtain

$$\omega^2(k) = \begin{cases} \left(1+\frac{1}{m}\right) - \sqrt{\left(1+\frac{1}{m}\right)^2 - \frac{4}{m}\sin^2(k\pi/N)} & \text{for } k = 0, \ldots, N-1, \\ \left(1+\frac{1}{m}\right) + \sqrt{\left(1+\frac{1}{m}\right)^2 - \frac{4}{m}\sin^2(k\pi/N)} & \text{for } k = N, \ldots, 2N-1. \end{cases} \tag{41}$$

The angular frequencies of the ZBM and BEMs are given as follows:

$$\omega^2(N/2) = 2, \tag{42}$$

$$\omega^2(3N/2) = 2/m, \tag{43}$$

$$\omega^2(N) = 2(1+1/m). \tag{44}$$

It is found that the displacement of particles in the ZBM and BEMs is uniform and nonzero. The normalized displacement of the particles in these modes is given by

$$q_j(t) = u_j \exp[i\omega(k)t], \tag{45}$$

where

$$u_j = \begin{cases} q_{2j-1} = N^{-1/2}(-1)^j, & \\ q_{2j} = 0 & \text{for } k = N/2, \\ q_{2j-1} = 0, & \\ q_{2j} = (Nm)^{-1/2}(-1)^j & \text{for } k = 3N/2, \\ q_{2j-1} = -m[Nm(1+m)]^{-1/2}, & \\ q_{2j} = [Nm(1+m)]^{-1/2} & \text{for } k = N. \end{cases} \tag{46}$$

Next, we consider the nonlinear equations of motion (34) and (35). Nonlinear equations of motion have solutions of the form $q_j(t) = u_j\psi(t)$. Substituting these solutions into (34) and (35), we obtain the equation for $\psi(t)$ as follows:

$$\frac{d^2\psi}{dt^2} + \sum_{r=1}^{p} \mu_{2r}(k)\psi^{2r-1} = 0, \tag{47}$$

where $\mu_{2r}(k)$ is a constant depending on k. The explicit expressions for the three modes are as follows:

$$\mu_{2r}(N/2) = 2K_{2r}N^{-(r-1)}, \tag{48}$$

$$\mu_{2r}(3N/2) = 2K_{2r}(Nm)^{-(r-1)}m^{-1}, \tag{49}$$

$$\mu_{2r}(N) = 2K_{2r}N^{-(r-1)}\left(\frac{1+m}{m}\right)^r. \tag{50}$$

Integrating (47), we obtain

$$\left(\frac{d\psi}{dt}\right)^2 + \sum_{r=1}^{p} \frac{\mu_{2r}}{2r}(k)\psi^{2r} = h, \tag{51}$$

where h is a positive constant which is in proportion to energy.

IV. STABILITY ANALYSIS

Let $\xi(t)$ be a small perturbation of the solution of (34) and (35). The variational equations of the system are given as follows:

$$\frac{d^2\xi_{2j-1}}{dt^2} + \sum_{r=1}^{p} \chi_{2r}(k)\psi^{2r-2}(2\xi_{2j-1} - \xi_{2j-2} - \xi_{2j}) = 0, \tag{52}$$

$$m\frac{d^2\xi_{2j}}{dt^2} + \sum_{r=1}^{p} \chi_{2r}(k)\psi^{2r-2}(2\xi_{2j} - \xi_{2j-1} - \xi_{2j+1}) = 0, \tag{53}$$

where $\chi_{2r}(k)$ is a constant depending on k and is given by

$$\chi_{2r}(N/2) = (2r-1)K_{2r}N^{-(r-1)}, \tag{54}$$

$$\chi_{2r}(3N/2) = (2r-1)K_{2r}(Nm)^{-(r-1)}, \tag{55}$$

$$\chi_{2r}(N) = (2r-1)K_{2r}N^{-(r-1)}\left(\frac{1+m}{m}\right)^{r-1}. \tag{56}$$

We introduce the new variables x_η, which denote small perturbations in the normal-mode coordinate. The variable transformations from ξ_j to x_η are given as follows:

$$\xi_{2j-1} = \sqrt{\frac{2}{N}}\sum_{\eta=0}^{2N-1} U_\eta x_\eta \sin\left((2j-1)\eta\pi/N + \frac{\pi}{4}\right), \tag{57}$$

$$\xi_{2j} = \sqrt{\frac{2}{N}}\sum_{\eta=0}^{2N-1} V_\eta x_\eta \sin\left(2j\eta\pi/N + \frac{\pi}{4}\right), \tag{58}$$

where U_η and V_η are the amplitudes of the ηth normal modes and are given as

$$U_\eta = 2\cos(\eta\pi/N), \tag{59}$$

$$V_\eta = 2 - \omega^2(\eta). \tag{60}$$

Note that the wave numbers of the acoustic perturbations are given as $0 \leqslant \eta < N$ and those of the optical perturbations are given as $N \leqslant \eta < 2N$.

By the variable transformation of ξ_j to x_η, we obtain the decoupled form of the variational equations

$$\frac{d^2x_\eta}{dt^2} + \left(\sum_{r=1}^{p} \chi_{2r}(k)\psi^{2r-2}\right)\omega^2(\eta)x_\eta = 0 \quad (0 \leqslant \eta < 2N). \tag{61}$$

By changing the scale as $\psi = h^{1/2p}\bar{\psi}$ and $t = h^{(1-p)/2p}\bar{t}$, Eqs. (47), (51), and (61) can be transformed into

$$\frac{d^2\bar{\psi}}{d\bar{t}^2} + \sum_{r=1}^{p} [\mu_{2r}(k) h^{r/p-1} \bar{\psi}^{2r-1}] = 0, \tag{62}$$

$$\frac{1}{2}\left(\frac{d\bar{\psi}}{d\bar{t}^2}\right)^2 + \sum_{r=1}^{p} \left(\frac{\mu_{2r}}{2r} h^{r/p-1} \bar{\psi}^{2r}\right) = 1, \tag{63}$$

$$\frac{d^2 x_\eta}{d\bar{t}^2} + \sum_{r=1}^{p} [\chi_{2r}(k) h^{r/p-1} \bar{\psi}^{2r-2}] \omega^2(\eta) x_\eta = 0. \tag{64}$$

In the high-energy limit $h \to \infty$, only the highest-order term in the summation of (62)–(64) becomes dominant, since $h^{r/p-1} \to \infty$ in the case of $r < p$. Therefore, applying $h \to \infty$ to (61), we find that only the highest-order term becomes dominant in the high-amplitude case. The monodromy matrix of (61) converges to that of the homogeneous equations. Thus, we can consider the equation

$$\frac{d^2 x_\eta}{dt^2} + \chi_{2p}(k) \psi^{2p-2} \omega^2(\eta) x_\eta = 0, \tag{65}$$

with

$$\frac{d^2\psi}{dt^2} + \mu_{2p}(k) \psi^{2p-1} = 0. \tag{66}$$

We can obtain the explicit form of the monodromy matrix of the variational equation (65) in the manner described in Sec. II. The stability parameter (5) can be written as

$$\lambda_{2p}(k, \eta) = \frac{\chi_{2p}(k) \omega^2(\eta)}{\mu_{2p}(k)}. \tag{67}$$

Next, we consider the characteristic multiplier $|\rho| \geqslant 1$ of (61). We can obtain ρ_{hom} for the homogeneous equation (65) as

$$\rho_{hom} = F_{2p}(\lambda_{2p}(k, \eta)) + \sqrt{\{F_{2p}(\lambda_{2p}(k, \eta))\}^2 - 1}, \tag{68}$$

where $F_{2p}(\lambda)$ is defined by (20). The characteristic multiplier ρ of inhomogeneous systems converges to ρ_{hom} as $h \to \infty$. Thus, we can describe the relation between ρ and ρ_{hom} as $\rho = \rho_{hom} + \epsilon(h)$, where $\epsilon(h)$ is a function of $\epsilon(h) \to 0$ as $h \to \infty$.

The characteristic exponent σ for (61) is given by $\sigma(k, \eta, h) = T^{-1}(h) |\rho|$. The period $T(h)$ is given by

$$T(h) = \oint_{\Gamma'} \frac{dw}{\sqrt{P(w)}}, \tag{69}$$

$$P(w) = 2h - \sum_{r=1}^{p} \frac{\kappa_{2r}(k)}{r} w^{2r}, \tag{70}$$

where Γ' is an anticlockwise path involving two real branch points of $\sqrt{P(w)}$. By introducing the variable transformation $w = h^{1/2p} w'$, $T(h)$ can be rewritten as

$$T(h) = h^{-(1/2-1/2p)} \oint_{\Gamma'} \frac{dw'}{\sqrt{2 - \frac{\kappa_{2p}(k)}{p} w'^{2p}}}. \tag{71}$$

The integrand of (71) is independent of h. Therefore, in the high-energy limit, σ is approximately given by

$$\sigma(k, \eta, h) \sim h^{1/2-1/2p}. \tag{72}$$

Considering σ is given by (23), it is found that σ is a monotonic increasing function in terms of F_{2p} in the case of unstable perturbations ($F_{2p} > 1$). Thus, we can discuss the magnitude of $\sigma(F_{2p}(\lambda_{2p}))$ by comparing the magnitude of $F_{2p}(\lambda_{2p})$.

In order to compare the magnitude of $F_{2p}(\lambda_{2p})$ and $\sigma(F_{2p}(\lambda_{2p}))$, we take the first derivative of $F_{2p}(\lambda_{2p})$ and obtain

$$\frac{\partial F_{2p}}{\partial \lambda_{2p}} = -\frac{2\pi}{\sin^2(\pi/2)} \frac{1}{\sqrt{(p-1)^2 + 4p\lambda_{2p}}} \times \sin\left[\frac{\pi}{p}\sqrt{(p-1)^2 + 4p\lambda_{2p}}\right]. \tag{73}$$

From (73), it is found that F_{2p} becomes maximum when $\lambda_{2p} = \lambda^*(d) = \{4p^2 d^2 - (p-1)^2\}/4p$ $(d = 1, 2, \ldots)$. The maximum value $F_{2p}(\lambda^*)$ is a constant given as

$$F_{2p}(\lambda^*) = \frac{2}{\sin^2(\pi/2p)} - 1. \tag{74}$$

Substituting (74) into (23), we obtain the upper bound of σ:

$$\sigma^* = T^{-1} \ln\left[\frac{\cos(\pi/2p) + 1}{\sin(\pi/2p)}\right]^2. \tag{75}$$

Note that, in some cases, the maximum σ is less than the upper bound σ^*, since λ^* can be outside the region of unstable perturbations, $s_{2p}(i)$ defined by (24). Some examples of the range of λ_{2p} are shown in the following subsections.

The normalized growth rate $\bar{\sigma}$ is defined as

$$\bar{\sigma}(k, \eta) = \lim_{h \to \infty} \frac{\sigma(k, \eta, h)}{\max_\eta \sigma(k, \eta, h)} = D^{-1} |F_{2p}(\lambda_{2p}(k, \eta)) + \sqrt{\{F_{2p}(\lambda_{2p}(k, \eta))\}^2 - 1}|, \tag{76}$$

where $D = \rho(F_{2p}(\lambda^*))$ is the upper bound of σ.

In the following subsections, we investigate the modulational instability of the ZBM and two BEMs in detail. Note that $\lambda_{2p}(k, \eta)$ and $\bar{\sigma}(k, \eta)$ satisfy the relation $\lambda_{2p}(k, \eta) = \lambda_{2p}(k, N - \eta)$ for the acoustic perturbations $(0 \leqslant \eta \leqslant N/2)$ and the relation $\lambda_{2p}(k, \eta) = \lambda_{2p}(k, 3N - \eta)$ for the optical perturbations $(N \leqslant \eta \leqslant 3N/2)$. We obtain the results in the cases $0 \leqslant \eta \leqslant N/2$ and $N \leqslant \eta \leqslant 3N/2$ in the following subsections.

A. ZBM ($k = N$)

From (50), (56), and (67), λ_{2p} of the ZBM is given as

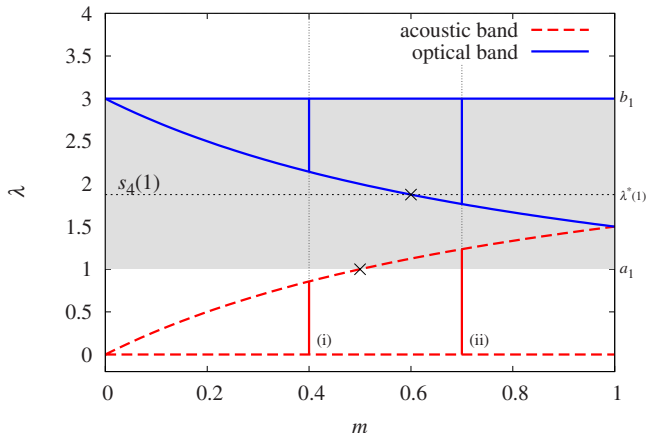

FIG. 2. (Color online) Range of the band of $\lambda_{2p}(N,\eta)$ versus m for $p=2$. The red (dashed) lines indicate the maximum and minimum values of $\lambda_{2p}(N,\eta)$ for the acoustic perturbations. The blue (solid) lines indicate those for the optical perturbations. The gray band shows the unstable regions $s_{2p}(i)$ bounded by a_j and b_j. The horizontal dashed line in $s_{2p}(i)$ indicates $\lambda^*(i)$, which corresponds to the upper bound of the growth rate σ^* defined in (75).

$$\lambda_{2p}(N,\eta) = \frac{2p-1}{2}\frac{m}{1+m}\omega^2(\eta). \tag{77}$$

Substituting (42)–(44) into (77), we obtain the range of λ_{2p} as

$$0 \leqslant \lambda_{2p}(N,\eta) \leqslant \frac{m}{1+m}(2p-1) \quad \text{for } 0 \leqslant \eta \leqslant N-1, \tag{78}$$

$$\frac{1}{1+m}(2p-1) \leqslant \lambda_{2p}(N,\eta) \leqslant 2p-1 \quad \text{for } N \leqslant \eta \leqslant 2N-1. \tag{79}$$

We can discuss the stability of perturbations on the basis of η by checking whether $\lambda_{2p}(N,\eta)$ lies in the region S_{2p} defined by (24) or not, since perturbations become unstable when $\lambda_{2p}(k,\eta) \in S_{2p}$. Figure 2 shows $\lambda_{2p}(N,\eta)$ versus m; this figure also shows the regions $s_{2p}(i)$.

The two red (dashed) lines in Fig. 2 indicate the minimum and maximum values of $\lambda_{2p}(N,\eta)$ $(0 \leqslant \eta < N)$ for the acoustic perturbations. The two blue (solid) lines indicate the minimum and maximum values of $\lambda_{2p}(N,\eta)$ $(N \leqslant \eta < 2N)$ for the optical perturbations. Therefore, $\lambda_{2p}(N,\eta)$ can take any value within the regions between the two red (dashed) lines or the two blue (solid) lines for a fixed m. The vertical lines (red and blue) between two red (dashed) lines and two blue (solid) lines in Fig. 2 indicate the examples of the ranges of $\lambda_{2p}(N,\eta)$ for two cases of m. The stability of perturbations can be analyzed by determining whether the *bands* of $\lambda_{2p}(N,\eta)$ are completely within the regions $s_{2p}(i)$, which are indicated by the gray band in Fig. 2. For example, in case (i), the band of the optical perturbations (blue line) is completely within the region $s_4(1)$. The band of the acoustic perturbations (red line) is completely outside the gray band. In case (ii), the band of the optical perturbations is within the region $s_4(1)$. The band of the acoustic perturbations is partially covered by $s_4(1)$. From these results, we find that the ZBM ($k=N$) is unstable in both cases (i) and (ii).

Next, we obtain the results of the stability analysis of the ZBM. By comparing (78) and (79) with (27) and (28), we have found that the upper bound of the band of the acoustic perturbations can be greater than $a_1=1$. Therefore, the band of $\lambda_{2p}(N,\eta)$ crosses the boundary between the stable region $\bar{s}_{2p}(1)$ and the unstable region $s_{2p}(1)$ once. On the other hand, the band of the optical perturbations remains within one unstable region $s_{2p}(1)$. As a result, the range of η of the unstable perturbations in the ZBM can be classified into the following two cases:

$$\text{(i) } N < \eta \leqslant \frac{3N}{2}(\text{optical}) \quad \text{for } 0 < m < \frac{1}{2(p-1)},$$

$$\text{(ii) } \eta_{c1}(a_1) < \eta < \frac{N}{2}(\text{acoustic}), \tag{80}$$

$$N < \eta \leqslant \frac{3N}{2}(\text{optical}) \quad \text{for } \frac{1}{2(p-1)} < m < 1,$$

where $\eta_{c1}(\lambda)$ is the critical wave number which is obtained by solving the equation $\lambda_{2p}(N,\eta_{c1})=\lambda$,

$$\eta_{c1}(\lambda) = \frac{N}{\pi}\sin^{-1}\left\{\frac{m+1}{2p-1}\frac{1}{m^{1/2}}[(2p-1)\lambda-\lambda^2]^{1/2}\right\}. \tag{81}$$

The bands labeled (i) and (ii) in Fig. 2 are examples of cases (i) and (ii) given in (80), respectively.

In Fig. 2, the line $\lambda=a_1$ and the upper bound $\lambda_{2p}(N,\eta)$ for the acoustic perturbations (red line) intersect at $m=1/2(p-1)$. Recall that a_i and b_i are defined as

$$a_i = i(i-1)p+i, \tag{82}$$

$$b_i = i(i+1)p-i. \tag{83}$$

Figure 3 shows $\bar{\sigma}$ for the cases $0<m<1/2(p-1)$ and $1/2(p-1)<m<1$; the acoustic perturbations can be stable or unstable depending on these conditions. The wave number $\eta_{\max}$ that gives the maximum $\bar{\sigma}$ is classified as the following two cases:

$$\eta_{\max} = \begin{cases} 3N/2 & \text{for } 0 < m < \dfrac{1-P}{P}, \\ \eta_1^* & \text{for } \dfrac{1-P}{P} < m < 1, \end{cases} \tag{84}$$

where η_1^* is obtained by solving the equation $\lambda_{2p}(N,\eta_1^*)=\lambda^*(1)$ for η_1^*,

$$\eta_1^* = \frac{N}{\pi}\sin^{-1}\left[P(1-P)\frac{(1+m)^2}{m}\right]^{1/2}, \tag{85}$$

and P is a function of p,

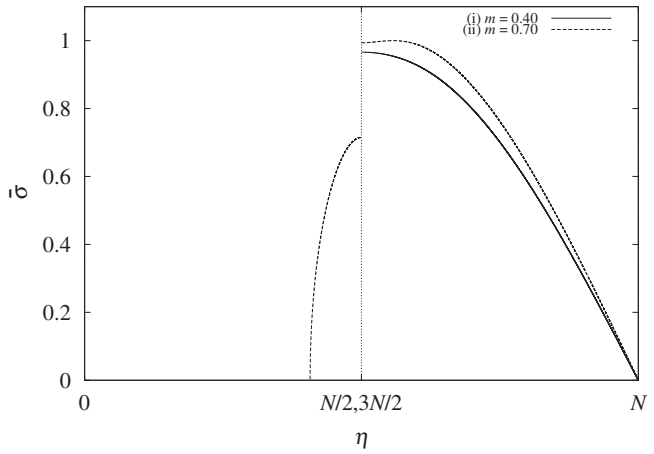

FIG. 3. The normalized growth rate $\bar{\sigma}$ of the perturbations in ZBM ($k=N$) for various values of m. The parameter m of cases (i) and (ii) corresponds to the parameter labeled in Fig. 2.

$$P(p) = \frac{(p+1)(3p-1)}{4p(2p-1)}. \tag{86}$$

In Fig. 2, the line $\lambda=\lambda_1^*(1)$ (horizontal dashed line) and the lower bound of band of $\lambda_{2p}(N,\eta)$ for the optical perturbations (blue solid line) intersect at $\frac{1-P}{P}$.

In summary, it is found that the ZBM is always unstable to arbitrary perturbations such as random noise.

B. BEM in optical band ($k=3N/2$)

From (49), (55), and (67), λ_{2p} is given by

$$\lambda_{2p}(3N/2,\eta) = \frac{2p-1}{2} m\omega^2(\eta). \tag{87}$$

Substituting (42)–(44) into (87), we obtain the range of $\lambda_{2p}(3N/2,\eta)$ as follows:

$$0 \leqslant \lambda_{2p}(3N/2,\eta) \leqslant (2p-1)m \quad \text{for } 0 \leqslant \eta \leqslant N-1, \tag{88}$$

$$2p-1 \leqslant \lambda_{2p}(3N/2,\eta) \leqslant (2p-1)(1+m) \quad \text{for } N \leqslant \eta \leqslant 2N-1. \tag{89}$$

Figure 4 shows $\lambda_{2p}(3N/2,\eta)$ versus m in the regions of unstable perturbations, $s_{2p}(i)$. It is found that (I) the upper bound of the acoustic band $(2p-1)m$ is smaller than $b_1=2p-1$ for all m and (II) the lower bound of the optical band $2p-1$ is equal to $b_1=2p-1$. Further, the upper bounds of the bands of both acoustic and optical perturbations cross the boundary between the stable region $\bar{s}_{2p}(i)$ and the unstable region $s_{2p}(i)$ once. The range of η of the unstable perturbations can be classified as following three cases:

(i) none for $0 < m < (2p-1)^{-1}$,

(ii) $\eta_{c2}(a_1) < \eta < \frac{N}{2}$ for $(2p-1)^{-1} < m < 3(2p-1)^{-1}$,

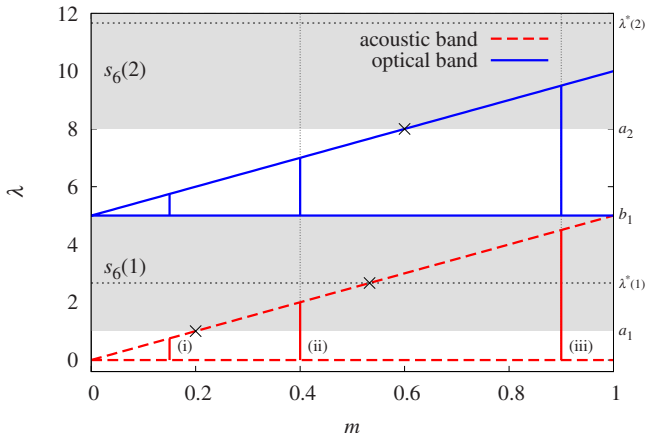

FIG. 4. (Color online) $\lambda_{2p}(3N/2,\eta)$ versus m for $p=3$. The definition of red (dashed) lines, blue (solid) lines, and gray bands is the same as that of Fig. 2.

(iii) $\eta_{c2}(a_1) < \eta < \frac{N}{2}$, $N < \eta < \eta_{c2}(a_2)+N$ for $3(2p-1)^{-1} < m < 1$, (90)

where $\eta_{c2}(\lambda)$ is the critical wave number obtained by solving the equation $\lambda_{2p}(3N/2,\eta_{c2})=\lambda$,

$$\eta_{c2}(\lambda) = \frac{N}{\pi}\sin^{-1}\left\{\frac{m^{1/2}}{2p-1}[\lambda(2p-1)(1+m)-\lambda^2]^{1/2}\right\}. \tag{91}$$

The bands labeled as (i), (ii), and (iii) in Fig. 4 represent the examples of cases (i), (ii), and (iii) given in (90), respectively. The upper bound of $\lambda_{2p}(3N/2,\eta)$ of the acoustic perturbations (red dashed line) and the line $\lambda=a_1$ intersect at $m=(2p-1)^{-1}$. The upper bound of $\lambda_{2p}(3N/2,\eta)$ of the optical perturbations (blue solid line) and the line $\lambda=a_2$ intersect at $m=3(2p-1)^{-1}$.

Note that the parameter $3(2p-1)^{-1}$ in (90) becomes equal to 1 in the case of the FPU-β system ($p=2$). Therefore, the optical perturbations in the BEM in the optical band are always stable in the FPU-β system.

Figure 5 shows $\bar{\sigma}$ in cases (ii) and (iii) of (90). The wave number $\eta_{\max}$ which gives the maximum growth rate for a fixed m is given as follows:

$$\eta_{\max} = \begin{cases} \text{none (always stable)} & \text{for } 0 < m < (2p-1)^{-1}, \\ N/2 & \text{for } (2p-1)^{-1} \leqslant m < P, \\ \eta_2^* & \text{for } P \leqslant m < 1, \end{cases} \tag{92}$$

where η_2^* is the wave number obtained by solving the equation $\lambda_{2p}(3N/2,\eta_2^*)=\lambda^*(1)$,

$$\eta_2^* = \frac{N}{\pi}\sin^{-1}\left[P\frac{1+m}{m} - P^2\frac{1}{m}\right]^{1/2}. \tag{93}$$

The upper bound of the acoustic perturbations (red dashed line) and the line $\lambda=\lambda^*(1)$ (horizontal dashed line) intersect at $m=P$.

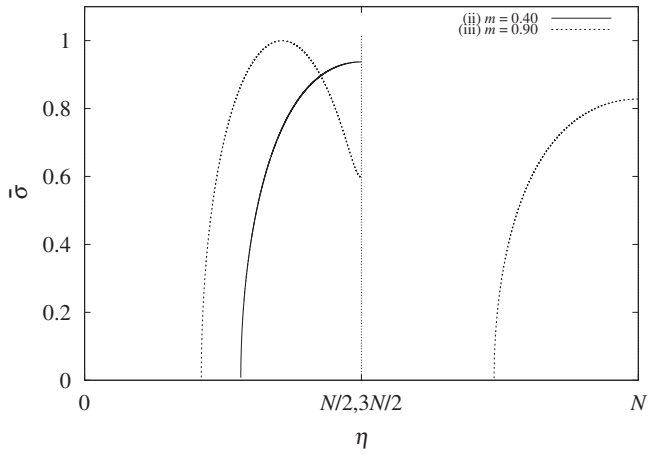

FIG. 5. The normalized growth rate $\bar{\sigma}$ of the perturbations in BEM in optical band ($k=3N/2$) for various values of m. The parameter m of cases (ii) and (iii) corresponds to the parameter labeled in Fig. 4.

In summary, it is found that the BEM ($k=3N/2$) is stable in the case of small m and is unstable otherwise.

C. BEM in acoustic band ($k=N/2$)

From (48), (54), and (67), λ_{2p} is given by

$$\lambda_{2p}(N/2,\eta)=\frac{2p-1}{2}\omega^2(\eta). \tag{94}$$

Figures 6 and 7 show $\lambda_{2p}(N/2,\eta)$ versus m for $p=2$ and $p=5$, respectively. In both figures, it is found that the band of $\lambda_{2p}(N/2,\eta)$ of the acoustic perturbations is in the regions $s(1)$ and $\bar{s}(1)$. The range of η of the unstable perturbations is given by

$$\eta_{c3}<\eta<N/2. \tag{95}$$

The critical wave number η_{c3} is obtained by solving the equation $\lambda_{2p}(N/2,\eta_{c3})=a_1(=1)$,

$$\eta_{c3}=\frac{N}{\pi}\sin^{-1}\left[\frac{1+m}{2p-1}-\frac{m}{(2p-1)^2}\right]^{1/2}. \tag{96}$$

In the case of optical perturbations, the range of $\lambda_{2p}(N/2,\eta)$ depends on m. Therefore, the regions $s_{2p}(i)$ and $\bar{s}_{2p}(i)$, which are covered by the band of $\lambda_{2p}(N/2,\eta)$, depend on m. Moreover, due to variation in the width of $\lambda_{2p}(N/2,\eta)$ and the widths of the regions $s_{2p}(i)$ and $\bar{s}_{2p}(i)$, the number of regions $s_{2p}(i)$ and $\bar{s}_{2p}(i)$ covered by the band of λ_{2p} can vary. Therefore, the stability of perturbations can be determined by comparing the widths of $s_{2p}(i)$ and $\bar{s}_{2p}(i)$ with the width of the band of $\lambda_{2p}(N/2,\eta)$. In summary, it is found that the range of η of the unstable perturbations is very complex and is given as follows.

Consider the cases $p<4$, which are shown in Fig. 6.

For $0<m<\frac{2p-1}{2(p+1)}$,

$$\text{(i}')\ N<\eta<\eta_{c4}(a_{i+1})+N$$

$$\text{for}\ \frac{2p-1}{a_{i+1}}<m<\frac{2p-1}{a_{i+1}-(2p-1)},$$

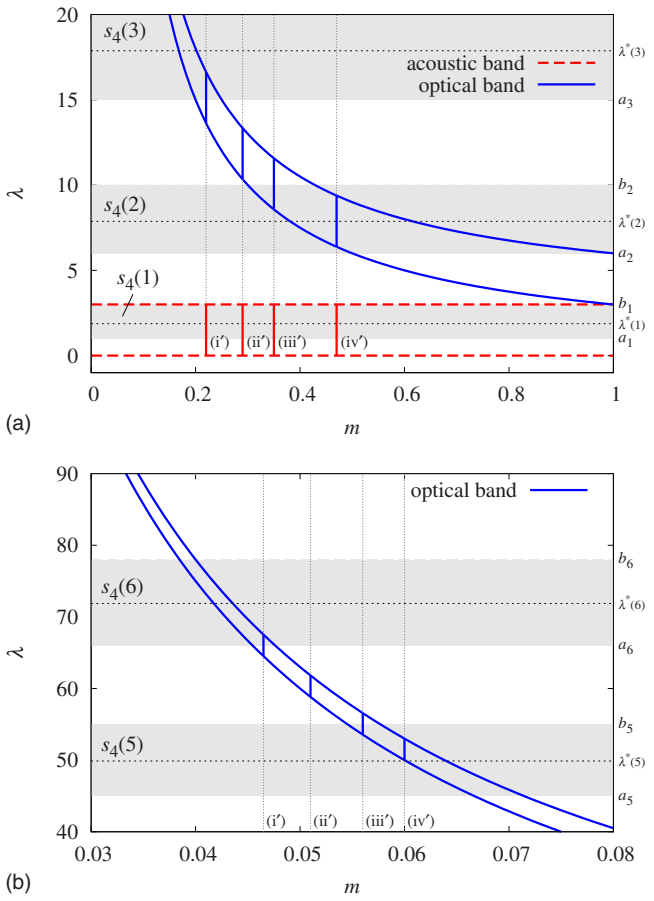

FIG. 6. (Color online) $\lambda_{2p}(N/2,\eta)$ versus m for $p=2$. The regions $s_{2p}(i)$ are also indicated. The definition of red (dashed) lines, blue (solid) lines, and gray bands is the same as that of Fig. 2. (a) and (b) show the variation in the band of $\lambda_{2p}(N/2,\eta)$ for the complete range of m and for $0.03<m<0.08$, respectively. In both cases, the bands of $\lambda(N/2,\eta)$ of the optical perturbations can be completely inside a single stable region $\bar{s}_{2p}(j)$ [see the bands labeled (ii)].

$$\text{(ii}')\ \text{none}\quad \text{for}\ \frac{2p-1}{a_{i+1}-(2p-1)}<m<\frac{2p-1}{b_i},$$

$$\text{(iii}')\ \eta_{c4}(b_i)+N<\eta<3N/2\quad \text{for}\ \frac{2p-1}{b_i}<m<\frac{2p-1}{b_i-(2p-1)},$$

$$\text{(iv}')\ N<\eta<3N/2\quad \text{for}\ \frac{2p-1}{b_i-(2p-1)}<m<\frac{2p-1}{a_i}$$

$$(i=2,3,\ldots). \tag{97}$$

For $\frac{2p-1}{2(p+1)}<m<1$,

$$N<\eta<\eta_{c4}(a_2)+N. \tag{98}$$

The bands labeled (i′)–(iv′) in Fig. 6 indicate examples in the range of $\lambda_{2p}(N/2,\eta)$ for the respective cases described in (97).

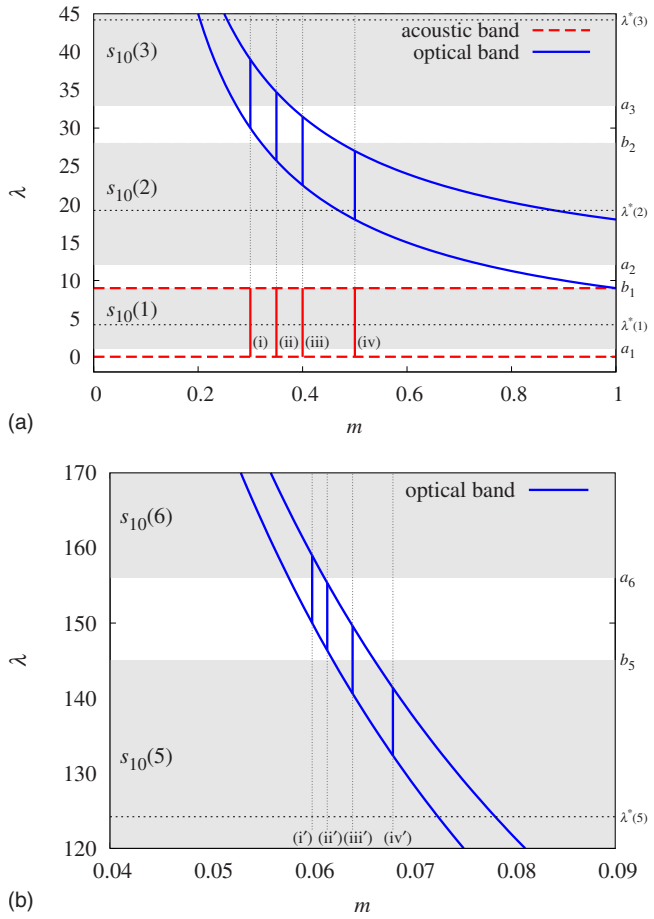

FIG. 7. (Color online) $\lambda_{2p}(N/2,\eta)$ versus m for $p=5$. The regions $s_{2p}(i)$ are also indicated. The definition of red (dashed) lines, blue (solid) lines, and gray bands is the same as that of Fig. 2. Each figure shows the variation in the band of $\lambda_{2p}(N/2,\eta)$ for (a) $m_1 < m < 1$ and (b) $0 < m < 1$, respectively. In case (a), the band of $\lambda_{2p}(N/2,\eta)$ of the optical perturbations can lie in two unstable regions [see the band labeled (ii)], while in case (b), $\lambda_{2p}(N/2,\eta)$ of the optical perturbations lies completely inside a single stable region $\bar{s}_{2p}(j)$ [see the band labeled$^{\lambda^*}$(ii′)].

Consider the case $p \geqslant 4$, which is shown in Fig. 7. For $0 < m < m_1$,

$$(\mathrm{i}')\ N < \eta < \eta_{c4}(a_{i+1}) + N \quad \text{for} \quad \frac{2p-1}{a_{i+1}} < m < \frac{2p-1}{a_{i+1}-(2p-1)},$$

$$(\mathrm{ii}')\ \text{none} \quad \text{for} \quad \frac{2p-1}{a_{i+1}-(2p-1)} < m < \frac{2p-1}{b_i},$$

$$(\mathrm{iii}')\ \eta_{c4}(b_i) + N < \eta < 3N/2 \quad \text{for} \quad \frac{2p-1}{b_i} < m < \frac{2p-1}{b_i-(2p-1)},$$

$$(\mathrm{iv}')\ N < \eta < 3N/2 \quad \text{for} \quad \frac{2p-1}{b_i-(2p-1)} < m < \frac{2p-1}{a_i} \quad (i = p-1, p, \ldots). \tag{99}$$

For $m_1 < m < \frac{2p-1}{2(p+1)}$,

$$(\mathrm{i})\ N < \eta < \eta_{c4}(a_{i+1}) + N \quad \text{for} \quad \frac{2p-1}{a_{i+1}} < m < \frac{2p-1}{b_i},$$

$$(\mathrm{ii})\ N < \eta < \eta_{c4}(a_{i+1}) + N, \eta_{c4}(b_i) + N < \eta < 3N/2 \quad \text{for} \quad \frac{2p-1}{b_i} < m < \frac{2p-1}{a_{i+1}-(2p-1)},$$

$$(\mathrm{iii})\ \eta_{c4}(b_i) + N < \eta < 3N/2 \quad \text{for} \quad \frac{2p-1}{b_{i+1}-(2p-1)} < m < \frac{2p-1}{b_i-(2p-1)},$$

$$(\mathrm{iv})\ N < \eta < 3N/2 \quad \text{for} \quad \frac{2p-1}{b_i-(2p-1)} < m < \frac{2p-1}{a_i} \quad (i = 2, 3, \ldots, p-2). \tag{100}$$

For $\frac{2p-1}{2(p+1)} < m < 1$,

$$N < \eta < \eta_{c4}(a_2) + N. \tag{101}$$

The bands labeled (i)–(iv) in Fig. 7(a) and (i′)–(iv′) in Fig. 7(b) indicate the examples of the range of $\lambda_{2p}(N/2,\eta)$ for the respective cases described in (99) and (100).

The critical wave number $\eta_{c4}(\lambda)$ is obtained by solving the equation $\lambda_{2p}(N/2,\eta_{c4}) = \lambda$,

$$\eta_{c4}(\lambda) = \frac{N}{\pi} \sin^{-1}\left\{ \frac{1}{2p-1} [\lambda(1+m)(2p-1) - m\lambda^2]^{1/2} \right\}. \tag{102}$$

For $p \geqslant 4$, there exists a critical mass m_1 given by

$$m_1 = \frac{2p-1}{(p-1)^3}. \tag{103}$$

The main difference between the cases $0 < m < m_1$ and $m_1 < m < 1$ for $p \geqslant 4$ is the width of the band of $\lambda_{2p}(N/2,\eta)$ of the optical perturbations and the width of the regions $s_{2p}(i)$. This difference leads to a difference in the range of η of the unstable perturbations—that is, (ii′) in (99) and (ii) in (100). Detailed discussions are given in Appendix B.

Figure 8 shows $\bar{\sigma}$ of the perturbations for four typical values of m corresponding to (i)–(iv) in Fig. 7(a).

Since the band of $\lambda_{2p}(N/2,\eta)$ of the acoustic perturbations covers the complete region of $s(1)$ as shown in Fig. 7, $\bar{\sigma}$ of the acoustic perturbations takes σ^*. The corresponding $\eta_{\max}$ is given by

$$\eta_{\max} = \frac{N}{\pi} \sin^{-1}[P(1+m) - P^2 m]^{1/2}. \tag{104}$$

In the case of the optical perturbations, on the other hand, $\bar{\sigma}$ and $\eta_{\max}$ show a complex change depending on m, shown in the right half of Fig. 8. For some values of m, $\sigma(\eta)$ can

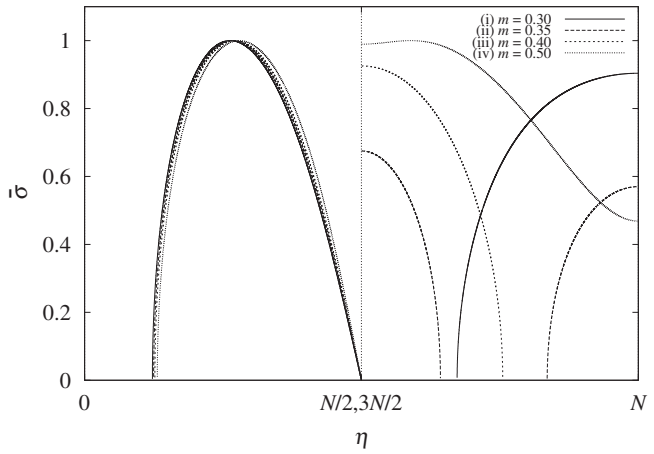

FIG. 8. The normalized growth rate $\bar{\sigma}$ of the perturbations in BEM in acoustic band ($k=N/2$) for various values m. The parameter m of the cases (i)–(iv) corresponds to the parameter labeled in Fig. 7.

take the value of σ^*. In other cases, $\sigma(\eta)$ is smaller than σ^* for all η of the optical perturbations, since λ^* lies outside the optical band of $\lambda_{2p}(N/2,\eta)$.

In summary, the BEM ($k=N/2$) is always unstable against arbitrary perturbations such as random noise.

D. Numerical simulations

In order to determine relation between the modulational instability and emergence of CBs in the diatomic lattice system, we carried out numerical simulations of the modulational instability in the FPU-β system. This system is regarded as a particular system of (30)—i.e., obtained by setting the parameter $p=2$ in (30). The stability analysis of this system is given in Appendix C. The Hamiltonian of the FPU-β system is

$$H=\frac{1}{2}\sum_{j=1}^{2N} m_j \dot{q}_j^2+\sum_{i=1}^{2N}\left[\frac{K_2}{2}(q_{j+1}-q_j)^2+\frac{K_4}{4}(q_{j+1}-q_j)^4\right]. \tag{105}$$

The parameters are $K_2=0.5$, $K_4=4$, and $N=256$. Initial displacement is given by the ZBM and two BEMs with small perturbation. The total energy of the system is same for all cases.

The results of the numerical simulation are shown in Figs. 9–11, which are examples of the cases classified in (C1)–(C3) in Appendix C, respectively. In Appendix C, it is stated that the ZBM and BEMs are unstable for all cases, except for the case of the BEM in the optical band in a system with $0<m<1/3$.

In the numerical results, all figures except Fig. 10(a) show the same behavior qualitatively. Initially, energy is uniformly distributed in the system. The ZBM or BEMs are modulated to form an array of breathers. Then, the breathers start moving and colliding with each other. The motion of the breathers is erratic. It is found that modulational instability leads to the excitation of CBs. In the case of Fig. 10(a), these processes do not occur. Hence, the BEM in this case is found to be stable.

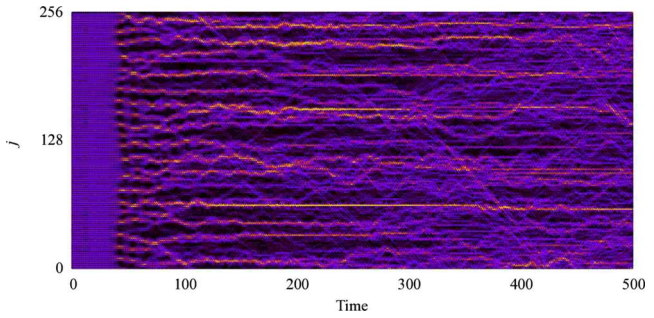

FIG. 9. (Color online) Temporal evolution of particle energy in BEM in acoustic band ($k=N/2$) in FPU-β lattice. Parameters are $m=0.2$, $K_2=0.1$, and $K_4=4$.

V. CONCLUSIONS

In this study, we analyzed the modulational instability of the BEMs and ZBM in a one-dimensional nonlinear diatomic

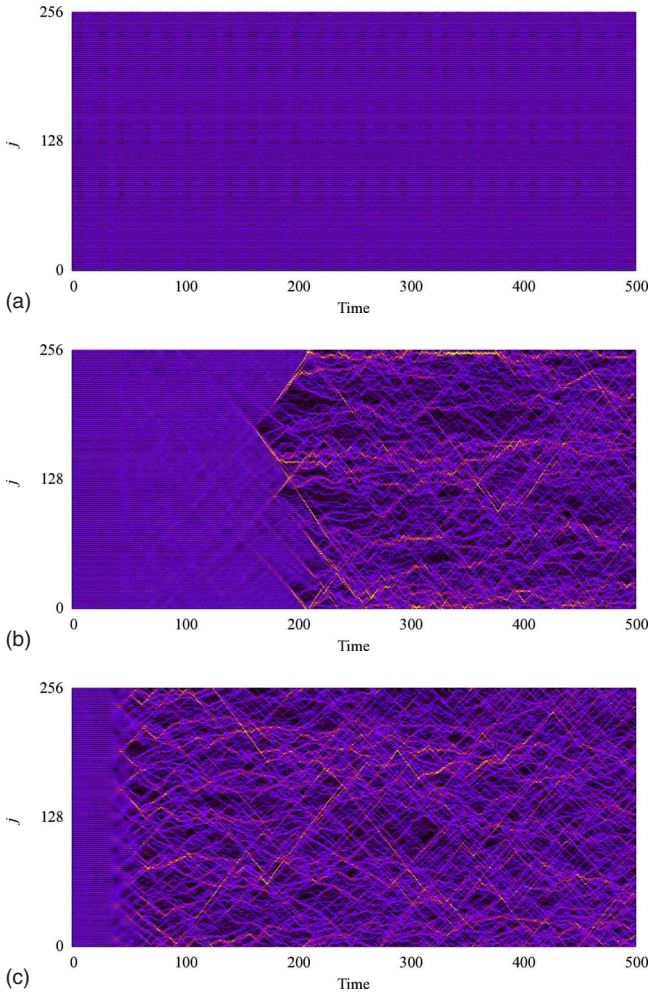

FIG. 10. (Color online) Temporal evolution of particle energy of BEM in optical band ($k=3N/2$). The parameter m is given as (a) $m=0.2$, (b) $m=0.5$, and (c) $m=0.8$. The other parameters K_2, K_4, and E are the same as those used in Fig. 9.

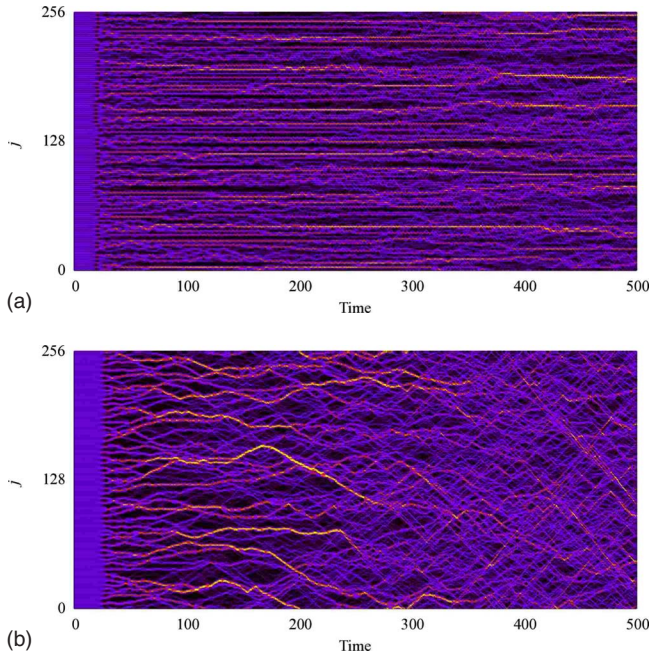

FIG. 11. (Color online) Temporal evolution of particle energy in ZBM ($k=N$). The parameter m is given as (a) $m=0.3$ and (b) $m=0.8$. The other parameters K_2, K_4, and E are the same as those used in Fig. 9.

lattice and obtained rigorous results. We obtained the growth rate σ of the perturbations and the wave number $\eta_{\max}$ that gives the maximum growth rate. It was found that stability depends on the mass ratio of heavy and light particles. The critical mass m_i at which the property of the modulational stability changed drastically was also obtained.

ACKNOWLEDGMENTS

This research was partly supported by a Grant-in-Aid for Young Scientists (B), No. 20760057, from MEXT, Japan.

APPENDIX A: DERIVATION OF THE GAUSS HYPERGEOMETRIC EQUATION

Consider the variable transformation

$$z = \left(\frac{\alpha_{2p}}{2ph}\right)[\phi(t)]^{2p}. \tag{A1}$$

Equations (3) and (6) can be rewritten as

$$\frac{d^2\phi}{dt^2} = -2ph[\phi(t)]^{-1}z, \tag{A2}$$

$$\left(\frac{d\phi}{dt}\right)^2 = 2h(1-z). \tag{A3}$$

Differentiating (A1) in terms of z and substituting (A2) and (A3), we obtain

$$\frac{dz}{dt} = \left(\frac{\alpha_{2p}}{h}\right)[\phi(t)]^{2p-1}\left(\frac{d\phi}{dt}\right) = 2pz[\phi(t)]^{-1}[2h(1-z)]^{1/2}, \tag{A4}$$

$$\frac{d^2z}{dt^2} = \left(\frac{\alpha_{2p}}{h}\right)\left\{(2p-1)[\phi(t)]^{2p-2}\left(\frac{d\phi}{dt}\right)^2 + [\phi(t)]^{2p-1}\left(\frac{d^2\phi}{dt^2}\right)\right\}$$
$$= 4phz[\phi(t)]^{-2}[(2p-1)-(3p-1)z]. \tag{A5}$$

Substituting (A4) and (A5) into

$$\frac{d^2\xi}{dt^2} = \frac{d^2\xi}{dz^2}\left(\frac{dz}{dt}\right)^2 + \frac{d\xi}{dz}\frac{d^2z}{dt^2}, \tag{A6}$$

we obtain

$$\frac{d^2\xi}{dt^2} = 4phz[\phi(t)]^{-2}\left\{2pz(1-z)\frac{d^2\xi}{dt^2} + [(2p-1)-(3p-1)z]\frac{d\xi}{dt}\right\}. \tag{A7}$$

Substituting (A1) and (A7) into (4) and after some calculations, we obtain the Gauss hypergeometric equation as

$$z(1-z)\frac{d^2\xi}{dt^2} + \left[\left(1-\frac{1}{2p}\right) - \left(\frac{3}{2}-\frac{1}{2p}\right)z\right]\frac{d\xi}{dt} + \frac{\lambda_{2p}}{4p}\xi = 0. \tag{A8}$$

APPENDIX B: DETAILED STABILITY ANALYSIS OF THE BEM IN THE ACOUSTIC BAND

Substituting (42)–(44) into (94), we obtain the range of λ_{2p} as

$$0 \leqslant \lambda_{2p}(N/2,\eta) \leqslant 2p-1 \quad \text{for } 0 \leqslant \eta \leqslant N-1, \tag{B1}$$

$$(2p-1)/m \leqslant \lambda_{2p}(N/2,\eta) \leqslant (2p-1)(1+1/m) \quad \text{for } N \leqslant \eta \leqslant 2N-1. \tag{B2}$$

In the case of the optical band of $\lambda_{2p}(N/2,\eta)$, we can discuss the stability by considering the width of the band of $\|\lambda_{2p}\|$ and the width of the regions $\|s(i)\|$ and $\|\bar{s}(i)\|$. The widths of these regions are given by

$$\|s(i)\| = 2i(p-1), \tag{B3}$$

$$\|\bar{s}(i)\| = 2i+1, \tag{B4}$$

$$\|\lambda_{2p}\| = 2p-1. \tag{B5}$$

By comparing $\|s(i)\|$, $\|\bar{s}(i)\|$, and $\|\lambda_{2p}\|$, it is found that

$$\|\lambda_{2p}\| < \|s(i)\| \quad \text{for } i > 1, \tag{B6}$$

$$\|\lambda_{2p}\| > \|\bar{s}(i)\| \quad \text{for } i < p-1, \tag{B7}$$

$$\|\lambda_{2p}\| \leqslant \|\bar{s}(i)\| \quad \text{for } i \geqslant p-1. \tag{B8}$$

These results indicate that for a fixed m, two stable regions $\bar{s}(l)$ and $\bar{s}(l+1)$ are never covered by the band of λ_{2p} for the optical perturbations at the same time. The two unstable regions $s(l)$ and $s(l+1)$, on the other hand, can be covered by the band of $\lambda_{2p}(N/2,\eta)$ in the case of $i<p-1$. Since the optical band $\lambda_{2p}(N/2,\eta)$ can cover the regions $\bar{s}_i$ for $i \geqslant 1$,

the condition $i<p-1$ is satisfied only if $r\geqslant 3$.

By solving the equation $(2p-1)/m=a_{p-1}$, we obtain m_1, which determines whether the band of λ_{2p} can cover the unstable regions $s(l)$ and $s(l+1)$ or not:

$$m_1=\begin{cases}1 & \text{for } p<3,\\ \dfrac{2p-1}{(p-1)^3} & \text{for } p\geqslant 3.\end{cases} \tag{B9}$$

As a result, the relation between the stable (unstable) regions and the perturbation band is classified as follows:

$$\lambda_{2p}\subset\begin{cases}\text{(i}'\text{) } \bar{s}_i\cup s_{i+1},\\ \text{(ii}'\text{) } \bar{s}_i,\\ \text{(iii}'\text{) } s_i\cup\bar{s}_i,\\ \text{(iv}'\text{) } s_i,\end{cases} \tag{B10}$$

for $m<m_1$,

$$\lambda_{2p}\subset\begin{cases}\text{(i) } \bar{s}_i\cup s_{i+1},\\ \text{(ii) } s_i\cup\bar{s}_i\cup s_{i+1},\\ \text{(iii) } s_i\cup\bar{s}_i,\\ \text{(iv) } s_i,\end{cases} \tag{B11}$$

for $m>m_1$.

Thus, we can calculate the range of η of the unstable perturbations, as in Sec. IV C.

APPENDIX C: STABILITY ANALYSIS IN THE FPU-β SYSTEM

In this section, we describe $\eta_{\max}$, which gives the maximum σ in the case of a FPU-β-type interaction ($p=2$). It should be noted that the parameter is exactly true only in the homogeneous case. However, even in the FPU-β system, which shows a harmonic interaction, we obtain the same results in the high-energy region.

1. BEM in the acoustic band ($k=N/2$)

For any m, $\eta_{\max}$ is given by

$$\eta_{\max}=\frac{N}{\pi}\sin^{-1}\left[\frac{5}{8}+\frac{15m}{64}\right]^{1/2}. \tag{C1}$$

2. BEM in optical band ($k=3N/2$)

$\eta_{\max}$ can be classified into three cases as follows:

$$\eta_{\max}=\begin{cases}\text{none(stable)}, & 0<m<1/3,\\ N/2, & 1/3<m<5/8,\\ \dfrac{N}{\pi}\sin^{-1}\left[\dfrac{5}{8}+\dfrac{15}{64m}\right]^{1/2}, & 5/8<m<1.\end{cases} \tag{C2}$$

3. ZBM ($k=N$)

$\eta_{\max}$ can be classified into two cases as follows:

$$\eta_{\max}=\begin{cases}3N/2, & 0<m<3/5,\\ \dfrac{N}{\pi}\sin^{-1}\left[\dfrac{15(1+m)^2}{64m}\right]^{1/2}+N, & 3/5<m<1.\end{cases} \tag{C3}$$

[1] E. Fermi, J. Pasta, and S. Ulam, in *Collected Papers of E. Fermi*, edited by E. Segré (University of Chicago Press, Chicago, 1965).
[2] S. Takeno, K. Kisoda, and A. J. Sievers, Prog. Theor. Phys. Suppl. **94**, 242 (1988).
[3] A. J. Sievers and S. Takeno, Phys. Rev. Lett. **61**, 970 (1988).
[4] V. M. Burlakov, S. A. Kiselev, and V. I. Rupasov, Phys. Lett. A **147**, 130 (1990).
[5] T. Cretegny, T. Dauxois, S. Ruffo, and A. Torcini, Physica D **121**, 109 (1998).
[6] K. Ullmann, A. J. Lichtenberg, and G. Corso, Phys. Rev. E **61**, 2471 (2000).
[7] V. V. Mirnov, A. J. Lichtenberg, and H. Guclu, Physica D **157**, 251 (2001).
[8] K. W. Sandusky and J. B. Page, Phys. Rev. B **50**, 866 (1994).
[9] T. Dauxois, R. Khomeriki, F. Piazza, and S. Ruffo, Chaos **15**, 015110 (2005).
[10] M. Leo and R. A. Leo, Phys. Rev. E **76**, 016216 (2007).
[11] K. Yoshimura, Phys. Rev. E **54**, 5766 (1996).
[12] K. Yoshimura, Phys. Rev. E **59**, 3641 (1999).
[13] K. Yoshimura, Phys. Rev. E **70**, 016611 (2004).
[14] Yu. S. Kivshar and M. Peyrard, Phys. Rev. A **46**, 3198 (1992).
[15] I. Daumont, T. Dauxois, and M. Peyrard, Nonlinearity **10**, 617 (1997).
[16] M. Aoki, S. Takeno, and A. J. Sievers, J. Phys. Soc. Jpn. **62**, 4295 (1993).
[17] O. A. Chubykalo and Yu. S. Kivshar, Phys. Rev. E **48**, 4128 (1993).
[18] R. Livi, M. Spicci and R. S. MacKay, Nonlinearity **10**, 1421 (1997).
[19] T. Cretegny, R. Livi, and M. Spicci, Physica D **119**, 88 (1998).
[20] P. Maniadis, A. V. Zolotaryuk, and G. P. Tsironis, Phys. Rev. E **67**, 046612 (2003).
[21] H. Yoshida, Physica D **29**, 128 (1987).